Hindawi
Structural Control and Health Monitoring
Volume 2023, Article ID 5497731, 17 pages
https://doi.org/10.1155/2023/5497731

Research Article

Superelastic Conical Friction Pendulum Isolator for Seismic Isolation of Bridges under Near-Fault Ground Motions

Wenzhi Zheng,[1,2] Ping Tan ,[1,2] Jian Li ,[3] Hao Wang ,[4] Yanhui Liu,[2] and Zhibin Xian[1]

[1]*School of Civil Engineering, Guangzhou University, Guangzhou 510006, China*
[2]*Key Laboratory of Earthquake Resistance Earthquake Mitigation & Structural Safety of Ministry of Education, Guangzhou University, Guangzhou 510006, China*
[3]*Department of Civil, Environmental and Architectural Engineering, University of Kansas, Lawrence, KS, USA*
[4]*Key Laboratory of C & PC Structures of Ministry of Education, Southeast University, Nanjing 210096, China*

Correspondence should be addressed to Ping Tan; ptan@gzhu.edu.cn and Hao Wang; wanghao1980@seu.edu.cn

Received 26 October 2022; Revised 28 February 2023; Accepted 11 March 2023; Published 4 April 2023

Academic Editor: Łukasz Jankowski

To improve the seismic performance of bridges, this study develops a novel superelastic conical friction pendulum isolator (SCFPI) by incorporating an improved conical friction pendulum isolator (CFPI) with shape memory alloy (SMA). The flat sliding function designed for the improved conical friction pendulum isolator is to enhance the adaptability under service loadings. The analytical model of the novel SCFPI is derived and the numerical model is developed within the OpenSees platform to investigate the hysteretic behavior under cyclic loadings. A cost-effective design method is proposed to design the SCFPI system for example bridges. The response mitigation efficacy of the novel SCFPI system is investigated using the optimum design parameters under near-fault ground motions. Several case studies are conducted to demonstrate the effectiveness of the novel SCFPI system and cost-effective design method. Results indicate that the cost-effective design method is particularly effective for parameter optimization of the novel SCFPI, which achieves effective mitigation for the displacement responses of the isolator and superstructure and also effectively controls the seismic force increment in piers. Case studies indicate the reliable re-centering capacity and mitigation efficacy of the SCFPI system for bridges under near-fault ground motions. The findings of this study contribute to upgrading structural resilience and promoting seismic applications as a reliable technical guidance.

1. Introduction

Seismic isolation has been identified as one of the most effective and practical seismic protection strategies for civil engineering structures [1–6]. Several studies have investigated the seismic performance of different types of isolation bearings, e.g., lead rubber bearing (LRB) [7, 8], pure-friction sliding isolator [9–11], and friction pendulum [12–18], which can effectively shift the fundamental period of the structures away from the predominant period of the seismic excitations, hence minimizing the seismically induced structural damage. Among these different types of isolation bearings, the friction-based sliding isolators with simple geometries [19], e.g., the friction pendulum and flat sliding isolator, have been widely investigated and are suitable for seismically isolated bridges [9, 14, 16, 17]. In particular, the friction pendulum combines both the re-centering and energy dissipation capacities using a spherical sliding surface and is particularly critical to protect the main members of the bridges from damage as well as a failure against strong earthquakes [14, 16, 17]. The seismic performance of bridges isolated by various isolation bearings has been validated by the real-world performance observed from several seismic events [20, 21].

The thermal movements observed in long-span bridges have attracked much concern [22, 23]. Large thermal deformations not only induce bearing damage under service loadings but also inevitably accelerate the function degradation of the isolators under seismic shaking [23, 24]. Due to the symmetrical nature of the thermal deformation, the movements induced in a spherical surface can lift up the

girder, negatively impacting the serviceability of the bridges underservice loadings (such as braking force). Also, the friction pendulum with constant curvature may inevitably introduce a constant isolation period to the seismically isolated structures [25–27]. As a result, resonance may be triggered when the isolation system is subjected to strong ground motions dominated by long-period components, such as near-fault earthquakes [26–28].

Several investigations have been focused on improving the passive adaptability of the traditional friction pendulum [25–31]. One example is the variable curvature friction pendulum, which can effectively improve the performance of structures [27, 31, 32]. In particular, the conical friction pendulum with an inclined plane tangent to the spherical surface can effectively control the maximum seismic force [30–32]. The component of the weight of the superstructure along the inclined plane provides stable re-centering capacity [33]. Also, the inclined plane with zero stiffness can effectively alleviate the structural resonance under near-fault ground motions [31–33].

Note that the flat sliding bearing is self-adaptable for both service and seismic loadings. Sliding not only enables the bridge to accommodate thermal movements but also makes the bridge less dynamically responsive to seismic excitations [1, 9, 10], hence effectively limiting the maximum shear of the bridge pier [1, 9]. For example, Zheng et al. [34] developed sliding-lead rubber bearing by incorporating the flat sliding bearing with lead rubber bearing in series for adaptability improvement. Note that the hysteretic behavior is less stable since the friction and yield characteristics of the sliding-LRB are responsive to the outside temperature [35], which shows unfavorable effect on its hysteretic mode. However, the re-centering members are always needed in flat sliding bearings for enhancing the re-centering capacity when employed in structures [1, 10]. It is accordingly necessary in terms of developing a versatile isolator with re-centering capacity and sustained adaptability for long-span bridges.

As an effective re-centering and damping measure, shape memory alloy (SMA) has been studied for its feasibility and effectiveness using in re-centering and energy dissipation devices [35–44]. Superelastic SMA has been widely investigated for the performance enhancement of bridges [35, 40–44]. For example, the SMA-cable-restrained high-damping rubber bearing developed by Fang et al. [43] has been first adopted in Datianba #2 bridge constructed in Yunnan Province, China, effectively demonstrating the real-world application of SMA for seismic protection of civil infrastructure. In view of the effectiveness of incorporating the SMA with different isolators for response mitigation [14, 42–52], the advantages of the SMA, i.e., superelastic re-centering and energy dissipation, show the promising prospect of application in structural seismic resilience enhancement [33, 43]. Particularly, several superelastic seismic isolators, e.g., superelastic flat sliding bearing [47–52] and superelastic friction pendulum [14, 53–57], in which the friction-based isolators are incorporated with the SMA wires/cables, have been investigated and seismic performances have been analytically and experimentally demonstrated. The SMA utilized in the superelastic friction pendulum is to enhance the re-centering capacity [14, 53]. Different from the friction pendulum, the superelastic flat sliding bearing requires a larger amount of SMA wires since the restoring stiffness of the flat pure-friction bearing is only provided by the SMA wires/cables [47–50].

As discussed previously, in comparison to the traditional friction pendulum, the conical friction pendulum may effectively mitigate the seismic shear demand by the inclined plane tangent to the spherical surface and avoid structural resonance [30–32]. On the other hand, the flat sliding bearing shows particularly better adaptability to thermal movements [9, 34] and avoids lifting up the superstructure than the friction pendulum bearing under service loadings. Meanwhile, the SMA is particularly effective for improving the re-centering capacity of the flat sliding bearing [49–52]. As a result, an isolator that combines the outstanding features of the conical friction pendulum, flat sliding bearing, and SMA shows immense potential for enhancing the sustained adaptability and seismic resilience of bridge structures. However, no literature is reported to incorporate the improved conical friction pendulum isolator and superelastic SMA for sustained structural adaptability and seismic resilience enhancement. Furthermore, when the friction pendulum system is excited under long-period components of near-fault earthquakes, the resonance phenomenon may occur [30–32]. In particular, it has been observed from several cases that traditional isolation systems with a constant period are especially sensitive to near-fault ground motions [58, 59], such as the unseating of the girder and isolator shifting observed from the Yematan Bridge under the 2021 Maduo Earthquake [59]. Near-fault ground motions should be paid great attention in terms of their effects on bridge performance.

To bridge the aforementioned research gap, this study proposes a novel superplastic conical friction pendulum isolator (SCFPI), which integrates the improved conical friction pendulum isolator (CFPI) and superelastic SMA device to enhance the sustained adaptability and seismic resilience of bridges. The numerical model of a bridge equipped with SCFPIs is created in the OpenSees platform [60], and the hysteretic behavior of the SCFPI is investigated under cyclic loadings. A cost-effective design method with a resilient concept is developed to capture the parameters of the SCFPI system for the example bridges. The proposed design method aims at achieving the optimum performance as well as controlling the amount of SMA. The suitability of the developed design method is verified by conducting parametric designs of bridges. The mitigation efficiency of the SCFPI system for bridges under near-fault ground motions is systematically demonstrated by conducting case studies and comparing the results with the benchmark responses.

2. The Proposed Novel SCFPI

2.1. Configuration of the SCFPI. The designed profile of the SCFPI consists of the improved CFPI and SMA devices, as shown in Figure 1. Particularly, the designed sliding surface is comprised of the flat surface R_0, spherical surface R_1, and inclined surface R_2 in series. The improved conical friction

pendulum isolator, termed as CFPI in this study, is different from the traditional conical friction pendulum without a flat surface [30, 31], is designed to prevent lifting up of the superstructure by being adaptable to the thermal movements. The spherical surface tangent to the flat surface is designed based on the initial isolation period [31]. Then, the inclined surface tangent to the spherical surface is designed to prevent the resonance and suppress the maximum shear of the isolator under earthquakes. Therefore, the sliding surface with various curvatures is designed to improve the sustained adaptability and seismic resilience against different excitations. The teflon-stainless steel interface is utilized for the sliding interface [61]. The teflon plate is designed to be embedded into the groove designed at the top and bottom surfaces of the slider.

The design profile of the SMA device shown in Figure 1 is adopted in this study [35, 46]. In particular, a symmetrically separate cross design suggested by Zheng et al. [35] is adopted for the SMA device, i.e., using the lower friction steel rings, the SMA device is wrapped around the improved CFPI in trilateral sides, and the ends are anchored by the steel clamps. Such an arrangement is also convenient for future inspection and replacement. To eliminate the unfavorable effects induced by the loading during construction, the SMA devices should be assembled after installing the CFPIs in predesigned positions and the major superstructure has been completely constructed [42]. Due to the feature of long-span bridges, the thermal movements of the bearing closely depend on the span length [22, 23]. As shown in Figure 1, the SMA devices are mainly designed to sustain the re-centering capacity and mitigate the residual isolator displacement induced in the longitudinal direction [23, 35]. The SMA devices function with the improved CFPI simultaneously under earthquakes.

By this design, the sliding surface with different curvatures aims at alleviating the resonance phenomenon under near-fault ground motions. The flat surface with the function of thermal movement accommodation also avoids the uplift of the girder. The inclined surface with zero frequency dissipates the seismic energy passed to the bridge and also effectively controls the peak seismic shear demand. The SMA device mainly contributes to the horizontal stiffness and re-centering force of the flat surface which does not have to restoring stiffness. The much lower yield modulus of the SMA also effectively alleviates the force increment in the bridge piers. Figure 2 shows the various working stages of the slider and SMA device of the SCFPI.

2.2. Mathematical Model of the SCFPI. Figure 3 shows the forces of the slider on various sliding surfaces of the SCFPI. The SCFPI achieves variable dynamic properties by the various sliding surfaces, including the flat surface R_0, spherical surface R_1, and inclined surface R_2. d_0 is the unilateral sliding displacement capacity of the flat surface. The curvature radius of the spherical surface R_1 and parameter d_b are important to define the geometry of the SCFPI. Five forces interact on the slider for a SCFPI with a symmetric sliding surface, as shown in Figure 3, which include the vertical loads W acting on the slider, the normal contact force N, the friction force F_f tangent to the surface, the force of the SMA device F_{si}, and the shear force F.

The flat sliding surface aims at accommodating thermal movements of the superstructure induced by service loadings (e.g., brake loading). When the slider is on flat surface R_0 ($d \le d_0$), as shown in Figure 3(a), the hysteretic force and vertical displacement of the novel SCFPI under service loadings are given as

$$\begin{aligned} F &= \mu W \bullet z + \sum F_{si}, \\ y_v(d) &= 0, \end{aligned} \tag{1}$$

where the friction coefficient μ are modelled using the modified viscoplasticity model [62], in which the maximum and minimum friction coefficients, μ_{max} and μ_{min}, are used to represent the model as follows:

$$\mu = \mu_{max} - (\mu_{max} - \mu_{min}) \bullet e^{-a|\dot{d}|}, \tag{2}$$

where $\dot{d}$ is sliding velocity, a is a constant related to vertical pressure and interface condition. The dimensionless parameter z satisfies

$$\dot{z} = \frac{1}{d_y}\left(A \bullet \dot{d} - \beta_0 \bullet |z|^{\eta_0} \bullet \dot{d} - \gamma_0 \bullet z \bullet |z|^{\eta_0 - 1} \bullet |\dot{d}|\right), \tag{3}$$

where the hysteretic dimensionless constants A, β_0, γ_0, and η_0 are related to mode transforming, the values of which are determined as $A = 1$, $\eta_0 = 2$, $\beta_0 = 0.1$ and $\gamma_0 = 0.9$ for the viscoplasticity model [62]. The value of the yield displacement d_y is selected as 1.0 mm [63].

As shown in Figure 3(b), when the slider moves on the spherical surface R_1 ($d_0 \le d \le d_b$), the hysteretic force and vertical displacement of the SCFPI are given as

$$\begin{aligned} F &= \frac{W}{R_1 \cos\theta}(d - d_0) + \mu W z + \sum F_{si}(1 - \mu z \tan\theta), \\ y_v(d) &= R_1 - \sqrt{R_1^2 - (d - d_0)^2}, \end{aligned} \tag{4}$$

where θ denotes the tangential angle of the spherical surface R_1. Once the displacement of the slider exceeds d_b, the sliding surface R_2 becomes an inclined surface tangent to the spherical surface R_1, as shown in Figure 3(c). The effect of the parameter d_b has been investigated in previous studies [30–32]. When the slider moves on the inclined surface R_2 ($d_b \le d$), the hysteretic force and vertical displacement of the SCFPI are given as

$$\begin{aligned} F &= \frac{W}{R_1 \cos\theta_1}(d_b - d_0) + \mu W z + \sum F_{si}(1 - \mu z \tan\theta_1), \\ y_v(d) &= c_1 + c_2\left(|d - d_0| - (d_b - d_0)\right), \end{aligned} \tag{5}$$

where θ_1 is the maximum tangential angle of the spherical surface R_1. The hysteretic model of the improved CFPI is shown in Figure 4(a). Q is the characteristic strength. The parameters c_1 and c_2 can be presented as

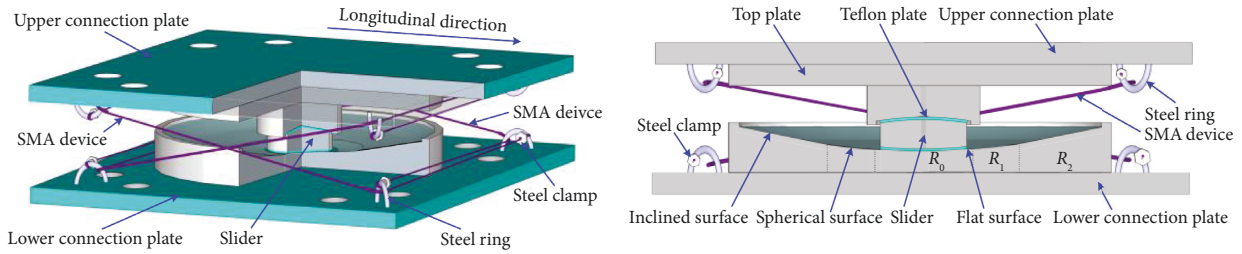

FIGURE 1: Configuration of the proposed novel SCFPI. (a) SCFPI configuration. (b) Cross-sectional view.

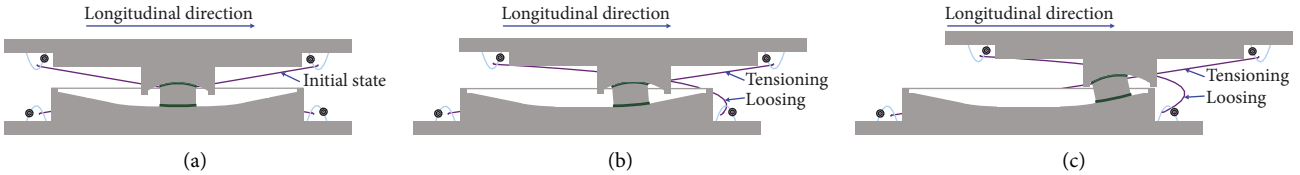

FIGURE 2: Working stages of the slider and SMA device of the SCFPI. (a) Flat surface R_0 (initial state). (b) Spherical surface R_1. (c) Inclined surface R_2.

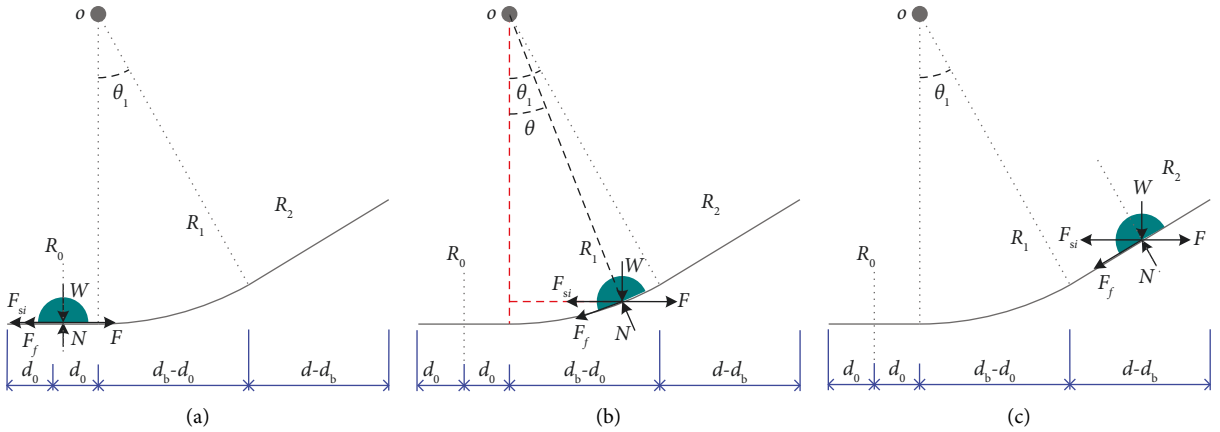

FIGURE 3: Forces of the slider on various sliding surfaces of the SCFPI. (a) $d \le d_0$, (b) $d_0 \le d \le d_b$, and (c) $d_b \le d$.

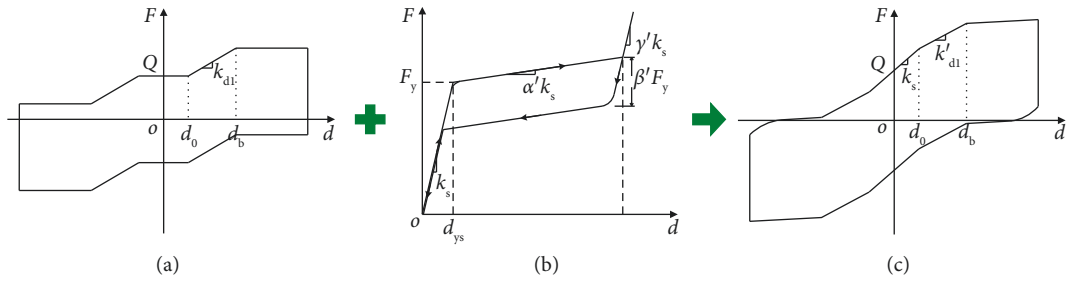

FIGURE 4: Hysteretic models of the novel SCFPI. (a) Improved CFPI model. (b) SMA model. (c) SCFPI model.

$$c_1 = R_1 - \sqrt{R_1^2 - (d_b - d_0)^2},$$
$$c_2 = \frac{(d_b - d_0)}{\sqrt{R_1^2 - (d_b - d_0)^2}}. \quad (6)$$

For the SMA device, the hysteretic force and the re-centering force are given as

$$F_{si} = \begin{cases} k_s d \cos\varphi, & d \le d_{ys}, \\ k_s d_{ys} \cos\varphi + \alpha' k_s (d - d_{ys}) \cos\varphi, & d > d_{ys}, \end{cases} \quad (7)$$
$$F_s = \left(1 - \beta'\right) k_s d_{sy} + \alpha' k_s (d - d_{ys}).$$

where φ is the angle of the SMA device in horizontal direction. β' is the hysteretic damping parameter, α' and γ' are the strain hardening ratio for phase transformation and martensite phase, respectively. F_y, d_{ys}, and k_s are the yield strength, yield displacement, and elastic stiffness, respectively. The hysteretic model of the SMA device is shown in Figure 4(b). Then, the hysteretic model of the SCFPI is achieved by combining the improved CFPI model with the SMA model, as shown in Figure 4(c). Though the friction force varies due to temperature change, the SCFPI provides a stable hysteretic mode for application in bridges in comparison to the isolators in previous studies [8].

The initial isolation period of the SCFPI system varies and depends on the radius of curvature R_1 [31] and the phase transformation stiffness of the SMA device. Due to a much lower stiffness of the SMA device after yielding, the predominant frequency of the SCFPI system is close to zero when the isolator displacement exceeds d_b. As a result, the initial isolation period of the SCFPI system is determined as

$$T_b = 2\pi \sqrt{\frac{W}{g\left(W/R_1 + \alpha' k_s\right)}}, \quad (8)$$

where g is the gravitational acceleration.

3. Cost-Effective Design Method

The SMA device, as shown in Figure 4(b), is designed to provide the re-centering capacity. Due to the much lower postyield stiffness, the yielding strength of the SMA device, F_y, is directly related to the effectiveness of providing re-centering performance and the contribution to the increment of the shear force of the SCFPI. On the other hand, the amount of the SMA wires depends on the value of F_y, which dictates the cost of the SMA wires. It is therefore needed to develop an effective method to design the optimal value of F_y by considering multiple indices.

A cost-effective design method, which defines the cost factor between the yield strength F_y and base shear (F_b) of the benchmark bridge, is proposed to achieve the optimal parameters of the SCFPI system under seismic shaking. Figure 5 shows the framework of the proposed design method. The focus of the method with resilience design concept is to mitigate the displacement responses and balance the increased shear to the piers by selecting the optimum cost factor, which is related to the yield strength F_y, i.e., the required amount of the SMA wires. To provide a technical guidance for practical design, the cost-effective design method is described in detail in the following subsection.

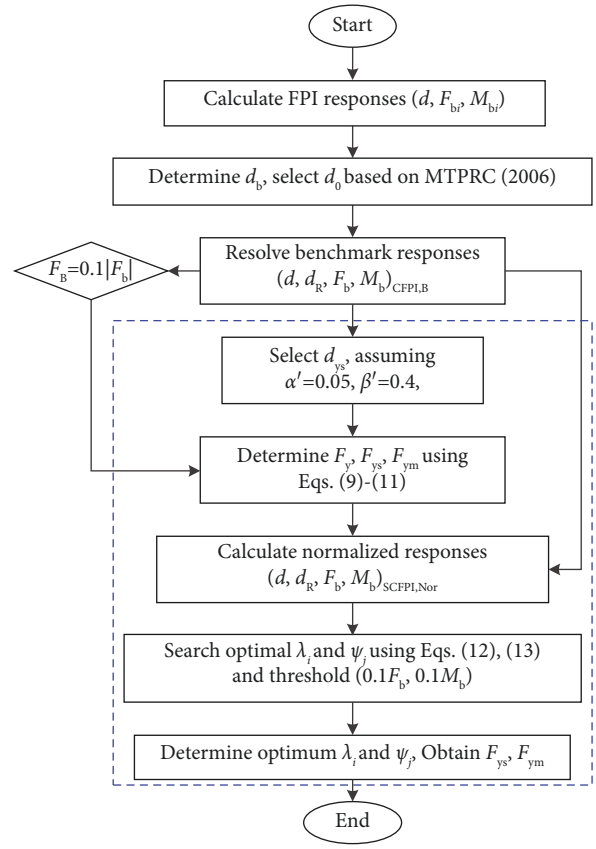

Figure 5: The framework of cost-effective design method.

3.1. Total Cost Factor λ_i. The yield strength of the SMA is closely related to the re-centering capacity of the SCFPI and the increased shear to the piers and reveals the needed amount of SMA. The total cost factor, termed as λ_i, is defined to establish the function relationship between the yield strength F_y and the defined reference force, i.e., the benchmark force F_B. To obtain the optimal design value of the yield strength, 0.1 times of the peak base shear in piers of the bridge with improved CFPIs is selected to define the benchmark force F_B. By defining the total cost factor λ_i, the yield strength F_y is obtained by

$$F_y = \lambda_i \cdot F_B, \quad (9)$$

where λ_i ranges from 0.1 to 1.0 ($i = 1, 2, \ldots$). The value of F_y corresponds to the utilized SMA amount for the SCFPI.

3.2. Local Cost Factor ψ_j. The increased shear in each pier is related to the yield strength of the SMA utilized in SCFPI. The optimal value of the yield strength of the SMA device for the middle and side SCFPIs may be different since the

corresponding loadings of the SCFPI in the side and middle piers are unequal. The local cost factor ψ_j is defined to search the optimal distribution of the SMA devices and aims at balancing the increased shear in each pier. By further defining the local cost factor ψ_j, the yield strength F_{ys} for the side SCFPI can be obtained by

$$F_{ys} = \psi_j \cdot F_y, \tag{10}$$

where ψ_j ranges from 0.0 to 1.0 ($j = 0, 1, 2, \ldots$). The value of F_{ys} corresponds to the utilized SMA amount for the side SCFPI. Furthermore, the yield strength F_{ym} for the middle one can be obtained by

$$F_{ym} = \left(1 - \psi_j\right) \cdot F_y. \tag{11}$$

According to equations (9)–(11), the dynamic responses of the SCFPI system with different cost factors is obtained. In particular, the normalized responses obtained based on that of the improved CFPI system, including the base shear (F_b) and moment (M_b) to the piers, girder displacement (d), and residual isolator displacement (d_R), are utilized as the evaluation indices to capture the optimum cost factors. The optimum cost factors are achieved when the evaluation indices satisfy the following criteria:

$$\max\left\{\Delta d_{k+1}, \Delta d_{R,k+1}\right\} < \min\left\{\Delta d_k, \Delta d_{R,k}\right\}, \tag{12}$$

$$\min\left\{\Delta d_{R,k}, \Delta d_k\right\} \leq \max\left\{\Delta F_{b,k,l}, \Delta M_{b,k,l}\right\}, \tag{13}$$

where the subscripts $k = 1, 2, \ldots, i-1$ and $l = 1, 2, \ldots, j$; Δ represents the change in the normalized responses. To endure the drifts of the piers to be within the elastic range and control the amount of the SMA wires, a threshold of the base shear increment corresponding to 10% of the benchmark values is selected.

4. The Bridge Model

4.1. Example Bridge. To investigate the performance of the novel SCFPI, an isolated bridge is selected as the example bridge in this study [34]. The configuration of the bridge is shown in Figure 6(a). The main components of the isolated bridge include the SCFPIs, continuous girder with three spans, and four reinforced concrete piers. The vertical loadings acting on the middle and side isolators are 15,986 kN and 3,582.6 kN, respectively, including the live load. Two isolators are used at the top of each pier. The bridge details can be found from a previous study [34, 42]. The parameters of the SCFPIs are summarized in Table 1.

4.2. Numerical Modeling. To demonstrate the seismic performance of the SCFPI system, the model of the selected bridge with SCFPIs is numerically developed in the OpenSees platform [60], as shown in Figure 6(b). The method suggested in a previous study [64] is employed to model the girder and piers utilizing a series of discretized elastic beam column elements connected by nodes. Based on the previous studies [34, 64], the piers are assumed to be elastic since one of the focuses of the cost-effective design method is to suppress the increase of the base shear in piers. The epistemic uncertainty [65] related to the assumptions in the bridge model is neglected. Further numerical validation for the assumption is also conducted based on the following numerical results. Half of the mass of the adjacent segments is assigned to the corresponding nodes of the beam elements. The characteristics of the cross sections of the piers and girder are calculated by the dimensions and material properties [34]. The boundary conditions of the piers are assumed to be fixed as suggested by the previous studies [42, 64]. The damping ratio for the piers is utilized as 2% [64].

The numerical model of the SCFPI is further investigated. Based on the hysteretic model shown in Figure 4, the hysteretic behavior of the improved CFPI is captured by combining the flat sliding element in Figure 6(c) with the elastic multilinear model in Figure 6(d), as shown in Figure 4(a). The flat sliding element in a vertical direction is considered as elastic. Note that the hysteretic model of the CFPI has been investigated and validated using testing results [30]. The hysteretic behavior of the SMA device is captured by incorporating the elastic multilinear model in Figure 6(e) with the elastic plastic element in Figure 6(f), as shown in Figure 4(b). The hysteretic model of the SCFPI is achieved by incorporating the improved CFPI model in parallel with the SMA model, as shown in Figure 4(c). Table 1 shows the experimentally obtained model parameters of the SCFPI, which include the friction coefficient obtained from the experiments of the Teflon-stainless steel interface [61] and the mechanical parameters of the Nitinol (NiTi, 51.0% Ti, and 49.0% Ni) wires [46].

The numerical model accuracy of the SCFPI is important for predicting dynamic responses of the seismically isolated bridge. The hysteretic responses of the SCFPI are further studied under cyclic loadings to verify the modeling method. As shown in Figure 7, the numerical results of the NiTi wires under cyclic loadings are compared to the experimental results [38, 46], in which the effective diameter and length of the utilized wires are 1 mm and 100 mm, respectively. It can be observed that the numerical and experimental results match well, which demonstrates the effectiveness of the modeling method for response prediction of the NiTi wire. In particular, Table 1 shows the model parameters of the SMA shown in Figures 6(e) and 6(f). Figure 7 also proves that the peak superplastic strain of the NiTi wire can reach 7%, which is also used in the numerical study.

Based on the hysteretic model of the improved CFPI and NiTi wire, the SCFPI for the bridge with the initial isolation period of 4.5 s is selected as a case study to reveal the hysteretic behaviors of SCFPI and its members. Particularly, the yield displacement and corresponding force of the SMA wires are defined as 30 mm and 50 kN, respectively. The yield strain of the NiTi wire is 0.8% [46], hence the effective superelastic displacement of the SMA device can reach 262.5 mm. The displacement amplitude and the sliding distance of the flat surface are selected as 150 mm and 30 mm, respectively.

Figure 8 shows the hysteretic curves of the improved CFPI, the SMA device, and the SCFPI under different types

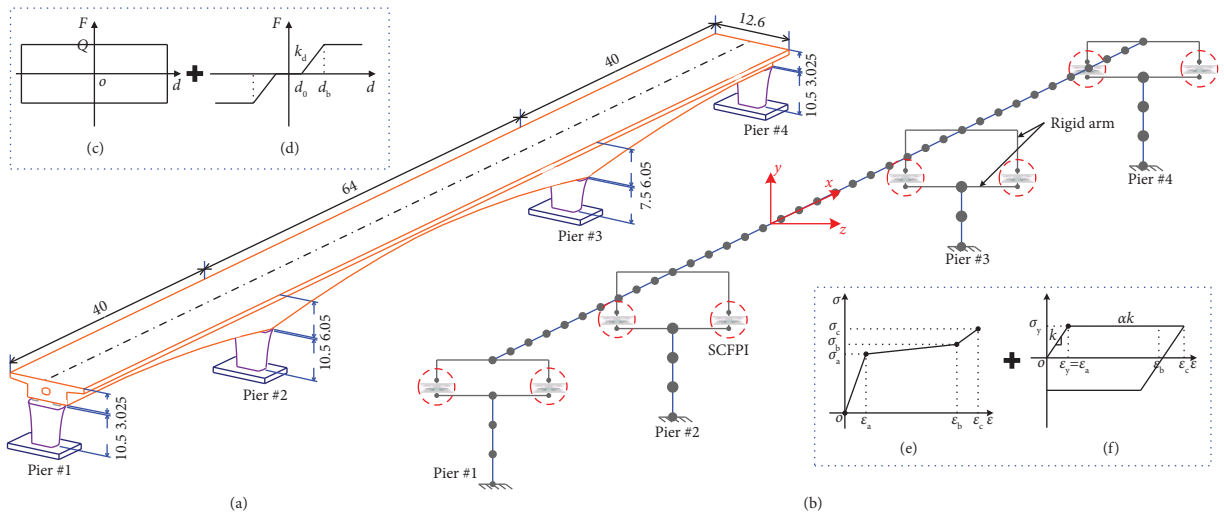

FIGURE 6: Configuration and numerical model of example bridge. (a) Bridge view (unit: m). (b) Numerical model of full-scale bridge. (c) Flat sliding model. (d) Elasticmultilinear model. (e) Elastic multilinear model. (f) Elastic plastic model.

TABLE 1: Model parameters of the SCFPIs [46, 61].

	Friction coefficients		Model parameters of SMA	
	Side	Middle	Elastic Multilinear model	Elastic Plastic model
P (MPa)	18.70	28.10	$\varepsilon_0 = 0,\ \sigma_0 = 0$ MPa	$\sigma_y = 91.7$ MPa
μ_{max} (%)	12.70	10.26	$\varepsilon_a = 0.8\%,\ \sigma_a = 249.5$ MPa	$\varepsilon_a = \varepsilon_y = 0.8\%$
μ_{min} (%)	4.49	3.13	$\varepsilon_b = 7.1\%,\ \sigma_b = 331.1$ MPa	$k = \sigma_y/\varepsilon_y$
a (s/mm)	0.020	0.022	$\varepsilon_c = 8\%,\ \sigma_c = 430.8$ MPa	$\alpha = 0$

of displacement loadings. It can be observed that the SMA device contributes to the horizontal stiffness of the flat surface significantly as well as the hysteretic damping. The purpose of including the SMA device aims at providing the re-centering capacity. The optimum yield strength of the SMA devices is closely related to the residual isolator displacement and hence needs to be designed using the cost-effective design method. As a result, the improved CFPI and SMA devices are first separately modelled, and then they are incorporated to create the numerical model of the SCFPI.

5. Selected Earthquake Records

The traditional friction pendulum system with constant isolation frequency is responsive to the long-period components of near-fault ground motions, which may trigger the resonance behavior [30–32]. Several studies have revealed that the effect of the near-fault ground motion on isolated structures is much more significant than the regular ground motions [43, 58, 59]. In particular, the Yematan Bridge experiences unrecoverable damage during the 2021 Maduo Earthquake, examples of damage include the typical shifting of bearing and failure of the girder [59]. According to the suggestions by Günay and Sucuoğlu [66], this study selects two groups of validated near-fault earthquakes from 15 different seismic events for effective investigation of the novel SCFPI system in a statistical sense. The selected records are summarized in Table 2. A two-step scaling method [34, 67], the advantage of which is to keep original frequency properties by scaling with constant factors, is

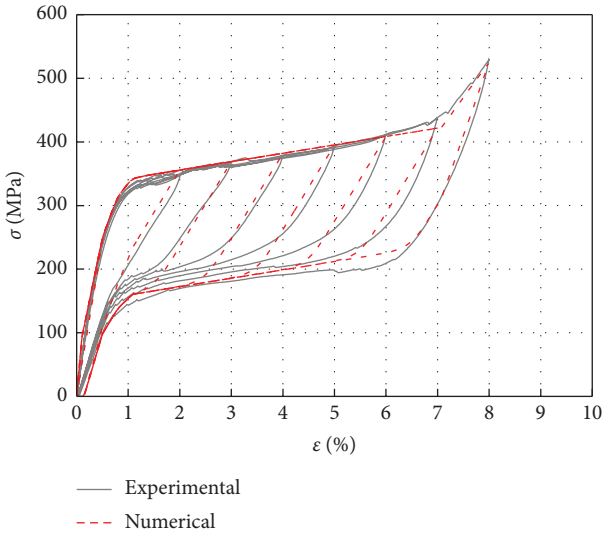

FIGURE 7: Numerical and test results of the NiTi wire.

utilized to match the target spectrum from MTPRC [68] with the scaled mean spectra, as shown in Figure 9. More information of the records can be found in a previous study [66]. To validate the effectiveness of the SCFPI system and the cost-effective design method, the records in Figure 9(a) are selected to design the SCFPI system for bridges. Then, all records in Figure 9 are utilized to demonstrate the seismic mitigation efficacy of the SCFPI system.

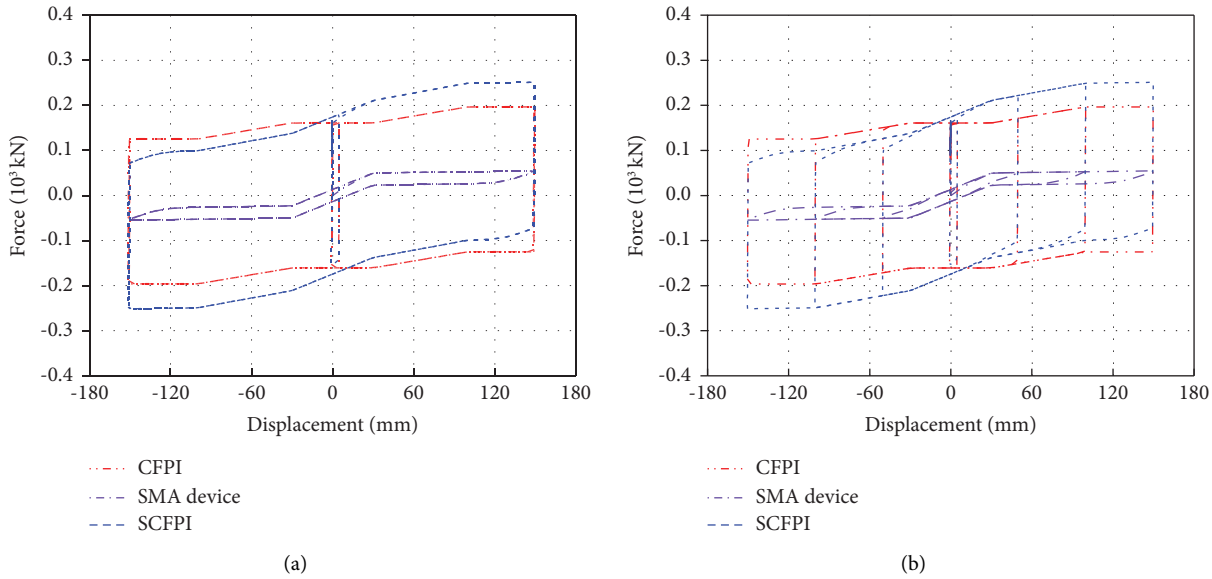

Figure 8: Hysteretic loops of the SCFPI and main components under cyclic loadings. (a) Constant amplitude. (b) Various amplitude.

Table 2: Ground motion record information [66].

Groups	n	M_w	V_s (m/s)	Soil type	D_R (km)
1	45	6.1–7.6	180–360	Stiff soil	<20
2	36	6.1–7.6	360–760	Soft rock	<20

M_w: moment magnitude; V_s: equivalent shear wave velocity; D_R: distance to rupture.

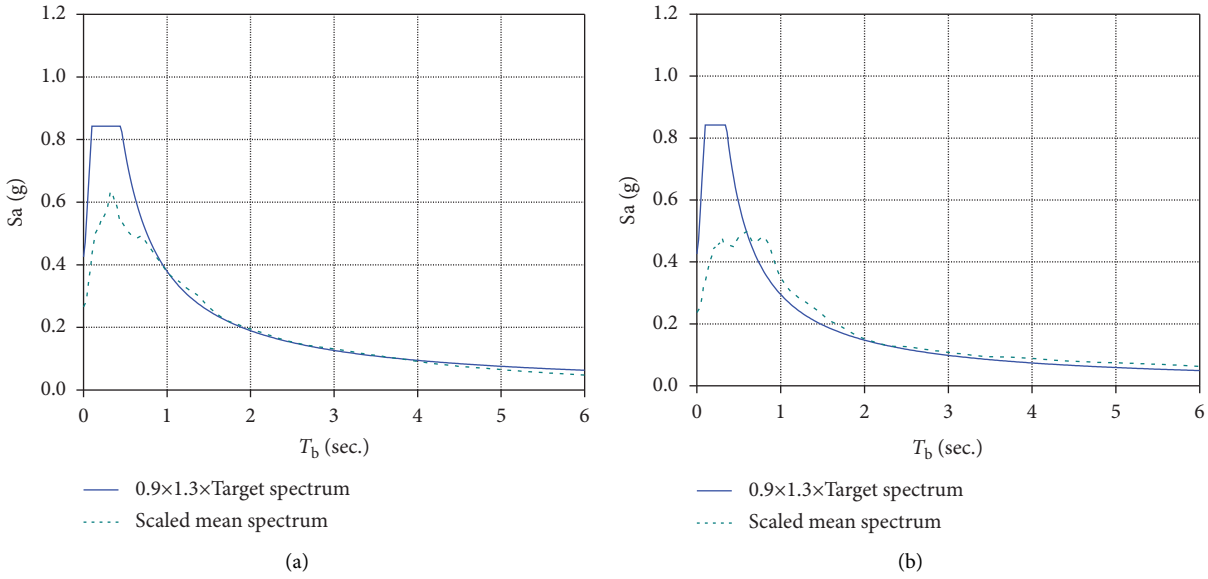

Figure 9: 5% damped target spectrum and matched mean spectrum. (a) Group #1. (b) Group #2.

6. Optimal Design of SCFPI Parameters

The cost-effective design method is used to design the SCFPI system for different bridges. The initial isolation period of the bridge corresponds to the stiffness of the spherical surface R_1 of the SCFPIs. The considered isolation periods range from 2.5 s to 4.5 s [14], which correspond to the first vibration mode of the bridges in the longitudinal direction. The radius of the curvature of the spherical surface of the side and middle SCFPIs are determined to be equal and is provided in Table 3. This is to prevent that the girder is asymmetrically uplifted under ground motions. The parameter d_b is determined by considering the peak displacement of the conventional friction pendulum system

Table 3: Optimum model parameters of SCFPIs.

T_b (s)	R_1 (m)	F_R (kN)	λ_i	ψ_j	F_{ys} (kN)	F_{ym} (kN)	A_{ys} (mm^2)	A_{ym} (mm^2)	n_{ys}	n_{ym}
2.5	1.6	450	0.4	0.6	108.0	72.0	316.5	211.0	403	269
3.0	2.2	440	0.4	0.6	105.6	70.4	309.5	206.3	395	263
3.5	3.0	435	0.5	0.6	130.5	87.0	382.5	255.0	487	325
4.0	4.0	435	0.5	0.6	130.5	87.0	382.5	255.0	487	325
4.5	5.0	435	0.5	0.6	130.5	87.0	382.5	255.0	487	325

n: amount of NiTi wire; A: total sectional area.

under selected earthquakes, in which the curvature radius is selected to be that of the spherical surface R_1. The friction coefficients shown in Table 1 are employed. As a result, the cost-effective design method aims at obtaining the optimum parameters of the SCFPI system.

According to the steps shown in Figure 5, the peak displacements of the friction pendulum system for the bridges are first investigated and then are selected to determine the parameter d_b, which corresponds to the peak displacement point of the spherical surface R_1. The sliding distance d_0 is determined by the MTPRC [69], the values of which are employed as 25 mm and 50 mm for the middle and side bearings [34], respectively.

Using the created bridge model, the benchmark response, i.e., the response of the bridge with improved CFPIs is investigated. Then, regarding the values of the sliding distance of the flat surface as the basis, the yield displacement (d_{ys}) of the SMA devices is selected as 30 mm [14, 47], which is also related to the peak superelastic displacement. To improve the applicability of the designed parameters, the parameters α', β' are assumed as 0.05 and 0.4 [70], which is statistically achieved based on the experimental results of various types of SMAs. To capture the alternative values of the yield strength, the increment of the total and local cost factors is selected as 0.1 in equations (9)–(11), i.e., the value of λ_i varies from 0.1, 0.2, . . ., 1.0, and that of ψ_j varies from 0.0, 0.1, . . ., 1.0. By conducting nonlinear dynamic analysis, the distribution of the dynamic responses of the SCFPI system with variable cost factors is achieved. The peak drift of all the piers is checked and the modeling assumption is validated by the fact that the peak value is far less than the elastic limit of 19.3 mm [42].

The example bridge with an initial isolation period of 4.5 s is employed as an example to conduct the optimization process of the SCFPI parameters. As shown in Figure 10, the normalized responses of the SCFPI system with different cost factors are investigated. The displacement responses of the SCFPI system are only dependent on the total cost factor, i.e., the total amount of the SMA wires. The peak girder displacement shows a closely linear reduction with the increase of the total cost factor. The residual isolator displacement shows a notably different variation trend and a significant reduction can be observed as the λ_i increases from 0.1 to 0.5, as shown in Figures 10(a) and 10(b). The force responses of the middle and side piers show much more difference, and the variation is closely dependent on the local cost factor, e.g., as the local cost factor increases, it can be observed that the base forces F_{bs} and M_{bs} increases, whereas the values of F_{bm} and M_{bm} reduce, as shown in Figures 10(c)–10(f). In Figure 10(d), as the total cost factor is close to 0.5, the local cost factor should be no less than 0.3. However, in Figure 10(e), the local cost factor needs to be no more than 0.6 as the total cost factor is close to 0.5. As discussed above, all the combinations of the total and local cost factors in the shadow shown in Figure 10 are alternate for the corresponding evaluation indices. Equations (12) and (13) are used to select the optimum combination of the cost factors by satisfying the evaluation criterion and the achieved optimal total and local cost factors are 0.5 and 0.6, respectively.

By conducting the design method in steps, the optimal total and local cost factors for the SCFPI system with different initial isolation periods are further achieved, as shown in Table 3. Also, the yield strength and amount of the SMA device can be further achieved. The cost factors reveal the optimal proportionality between the base shear in piers of the benchmark bridge with improved CFPIs and the yield strength of the SMA device, hence the optimal values of the cost factors are also adaptable for the SCFPI system utilized in other bridges.

7. Case Study

Case study is conducted to discuss the performance of the SCFPI system and the effectiveness of the cost-effective design method. The SCFPI system for the example bridge is designed for different isolation periods. In particular, the NiTi (51.0% Ti and 49.0% Ni) wire with a diameter of 1 mm is utilized to design and fabricate the SMA device. The experimental results are used to capture the model parameters of the SMA for numerical study. In Figure 7, the experimental hysteretic responses show that the superelastic strain is more than 7%, which is selected as the threshold in modeling the SMA device. The main purpose is to limit the force increment induced by the strain hardening of the SMA device in the martensite phase. According to the mechanical properties of the NiTi wires, as the superelastic strain is 7%, the effective superelastic displacement can reach 262.5 mm for a yield displacement of 30 mm. Figure 11 shows the designed dimensions of the novel SCFPI. The flat surface is designed to accommodate the thermal movements, the initial values of which are employed as 27.4 mm and 13.1 mm for side and middle SCFPIs [34, 42], respectively. The initial movements show symmetric features for the bearing in symmetric positions.

To demonstrate the seismic mitigation efficacy of the SCFPI system, the seismic responses of the bridge with SCFPIs are investigated and compared with the benchmark responses. The typical time history responses of the example bridge with an initial isolation period of 4.5 s under the Kocaeli earthquake (Yarimca) are compared, as shown in Figure 12. In Figure 12(a), the SCFPI system enhances the re-centering capacity significantly and reduces the girder displacement with an amplitude of 35.0%. The peak base shear in piers fluctuates slightly, as shown in Figure 12(b).

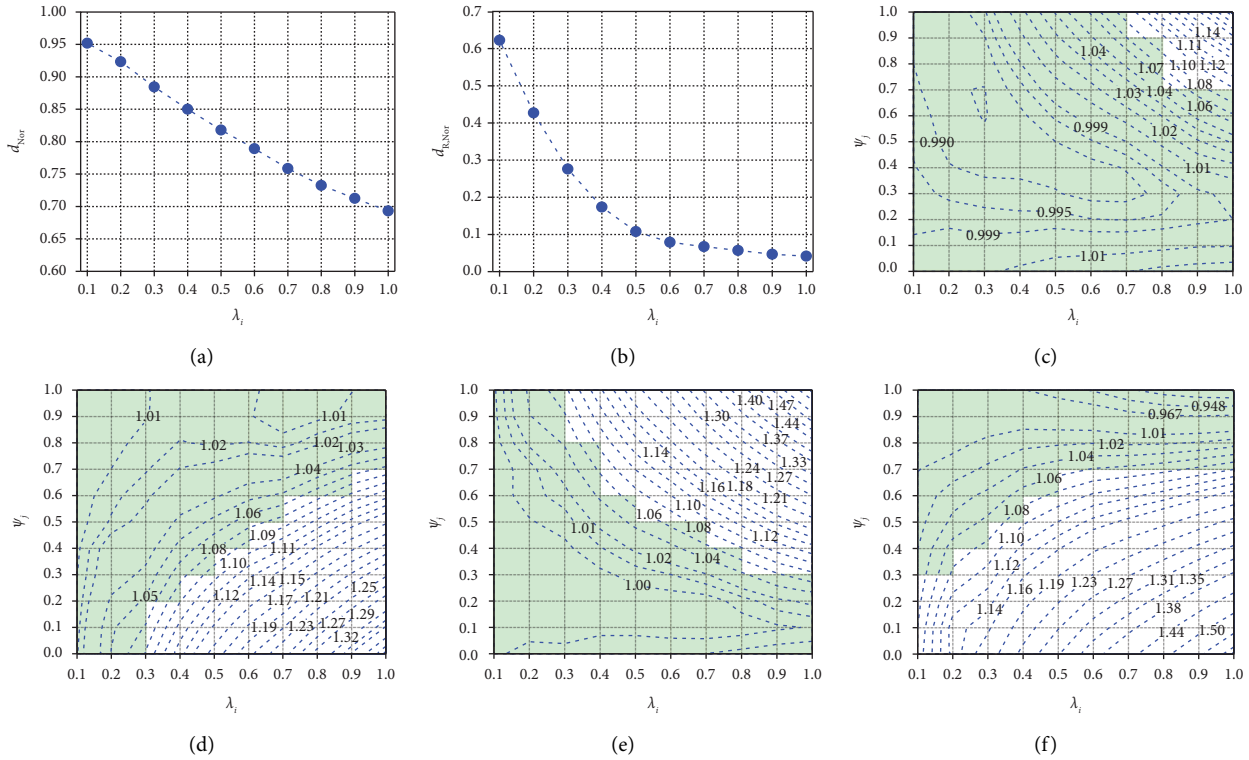

Figure 10: Normalized response variations with total and local cost factors. (a) d_{Nor}. (b) $d_{R,\text{Nor}}$. (c) $F_{\text{bs,Nor}}$. (d) $F_{\text{bm,Nor}}$ of pier #2. (e) $M_{\text{bs,Nor}}$. (f) $M_{\text{bm,Nor}}$ of pier #3.

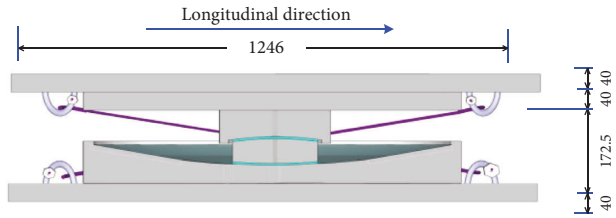

Figure 11: Designed dimensions of the novel SCFPI (unit: mm).

The typical dynamic responses of the SCFPIs at each pier are further compared. Due to the thermal movements of the side and middle SCFPIs, the hysteretic responses of the SCFPI in each pier are particularly different. As shown in Figure 13, the girder displacement reduces significantly. The energy dissipation capacity of the side SCFPI benefiting from the SMA device increases significantly since the utilized amount of the NiTi wires in the side SCFPI is more than that in the middle one. The shear of the side isolator also increases due to the contribution of the elastic stiffness of the SMA device.

As shown in Figures 14 and 15, the typical peak responses of the bridges with SCFPIs are investigated under the selected near-fault ground motions and the response distribution is compared with the benchmark values. In particular, in comparison to the benchmark response, the peak girder displacement and residual isolator displacement show a significant reduction trend. The SCFPI incorporating with the SMA device effectively enhances the re-centering capacity and the damping contribution also benefits the girder displacement mitigation, as shown in Figures 14(a), 14(b), 15(a), and 15(b). In some cases, the displacement responses of the SCFPI system show a slightly increase or little change. The possible reason is that the employed SMA devices contribute to changing the stiffness of the SCFPI system.

The base forces in piers show a similar trend, e.g., the base shear and bending moment vary closely to the diagonal line, which reveals that the cost-effective design method can effectively control the increments of the piers, as shown in Figures 14(c)–14(f). This is because the superelasticity of the SMA is utilized to enhance the re-centering capacity. The shear increment is suppressed by controlling the yield strength of the SMA device using the cost-effective design method. The contribution to the post-yield stiffness of the SMA device is slight. Hence, the base forces of the piers show slight fluctuations around the isoline, as shown in Figures 15(c)–15(f).

This study employs the scaled seismic records by matching the mean spectrum based on a two-step spectral

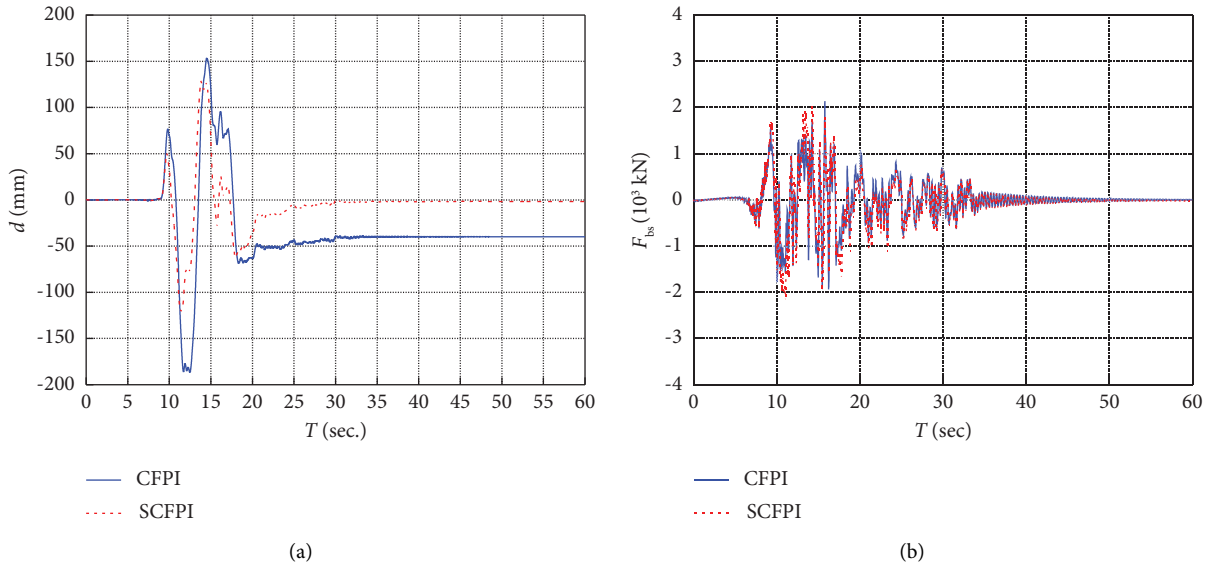

Figure 12: Time history responses of the SCFPI system under the Kocaeli earthquake.

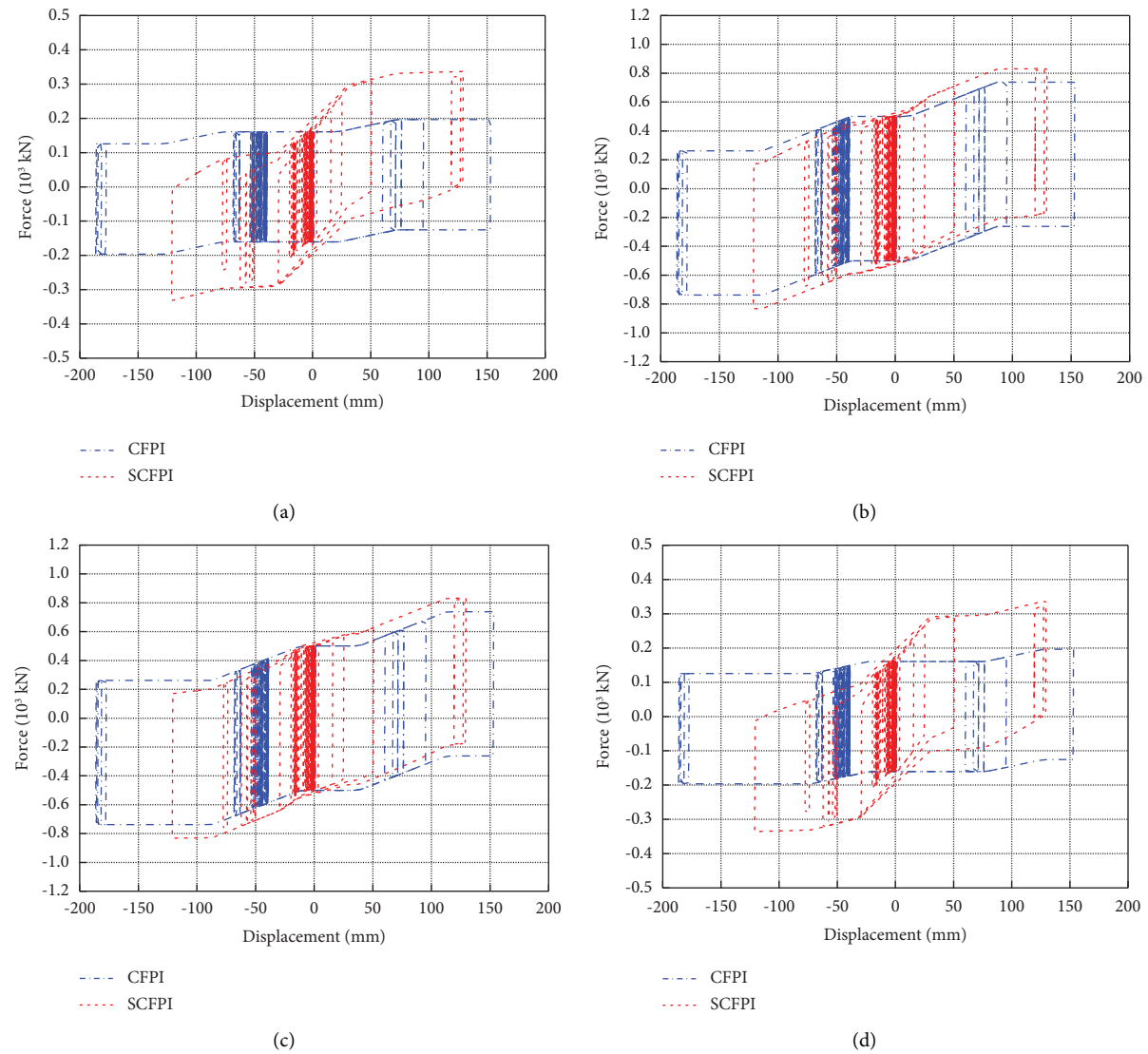

Figure 13: Hysteretic responses of the SCFPI system under the Kocaeli earthquake. (a) Isolator #1. (b) Isolator #2. (c) Isolator #3. (d) Isolator #4.

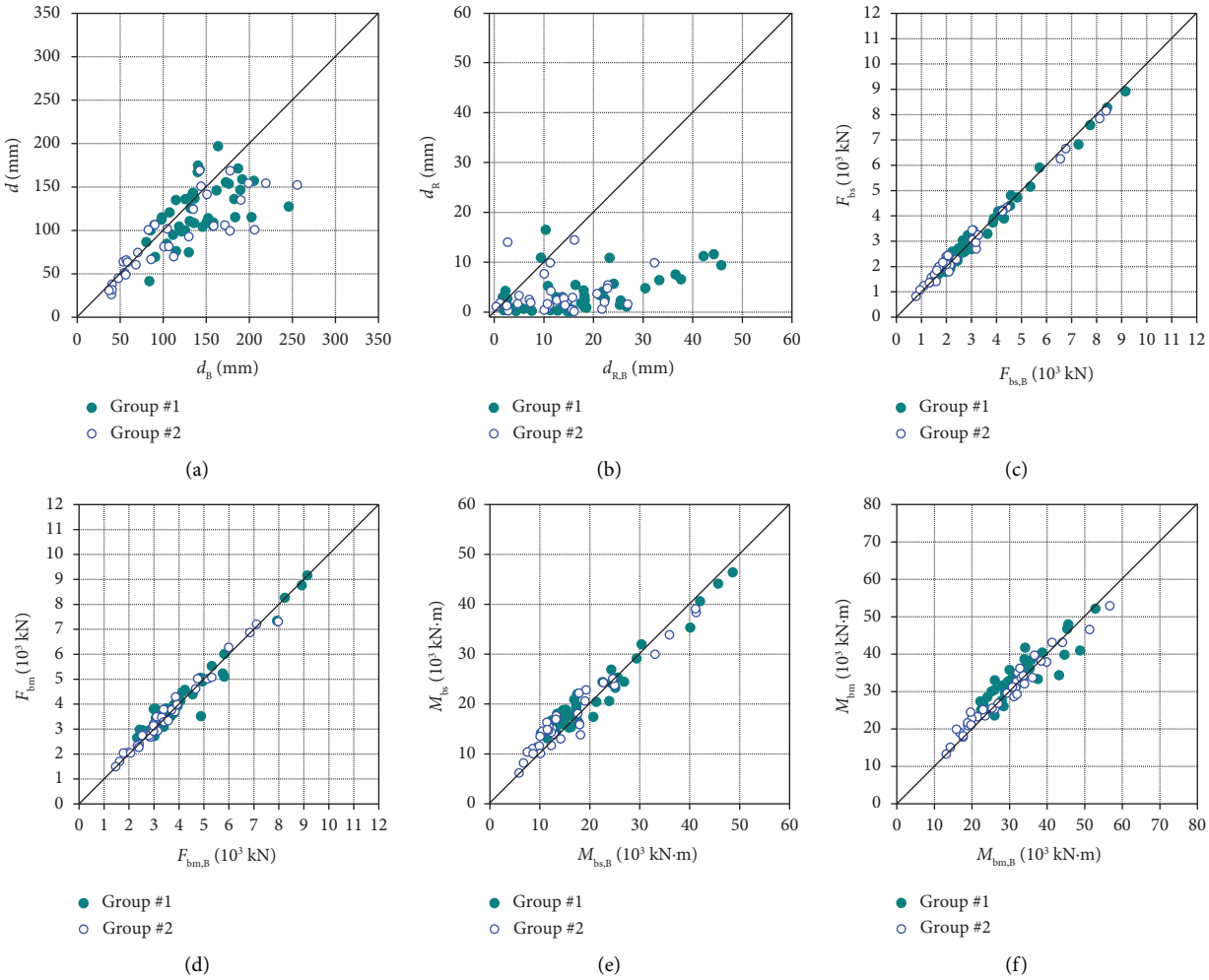

FIGURE 14: Response comparisons of SCFPI system with initial isolation period of 3.0 s, (a) d. (b) d_R. (c) F_{bs}. (d) F_{bm} in pier #2. (e) M_{bs}. (f) M_{bm} in pier #2.

matching method, hence the normalized mean responses are more reliable indices for the effectiveness evaluation of the SCFPI system. Particularly, the normalized mean responses of the SCFPI system is achieved using the benchmark responses of the example bridges with different initial isolation periods. Figure 16 provides the normalized mean values and variations of the SCFPI system under selected seismic records. Compared with the benchmark values, it can be observed that the peak girder displacement shows a relatively obvious reduction ranging from 13.4% to 17.4% shown in Figure 16(a) and ranging from 14.5% to 26.1% shown in Figure 16(b). By comparing to the girder displacement, the residual isolator displacement is more significantly mitigated, e.g., the reduction shown in Figure 16(a) ranges from 78.2% to 86.4%, and that shown in Figure 16(b) ranges from 71.2% to 85.9%. The results demonstrate that the designed SMA devices can effectively enhance the re-centering capacity of the SCFPI system. On the other hand, the maximum of the force increments in piers is 8.6% shown in Figure 16(a) and 7.3% shown in Figure 16(b), which are all suppressed to be less than 10%. The normalized girder displacement, residual isolator displacement, and the base forces demonstrate the control efficacy of the SCFPI system designed by the suggested method.

Due to the hysteretic damping characteristics of the NiTi wire, the SMA device also contributes to the damping capacity of the SCFPI system under near-fault earthquakes. Due to the larger local cost factor for the side isolator, the damping enhancement of the side isolator is more significant than that of the middle one, e.g., the damping increment of the side isolator ranges from 13.8% to 25.5%, whereas that of the middle isolator is relatively marginal, as shown in Figure 16(a). The damping increments of the side and middle isolators shown in Figure 16(b) are much smaller and show a similar trend as that shown in Figure 16(a). This is because the peak displacement of the SCFPI system under group #2 records is relatively smaller than that under group #1 records. The hysteretic damping contribution achieved from the SMA device deformed in phase transformation is marginal. As discussed above, the designed SCFPI system is an effective measure to enhance the response control efficacy of bridges. The case

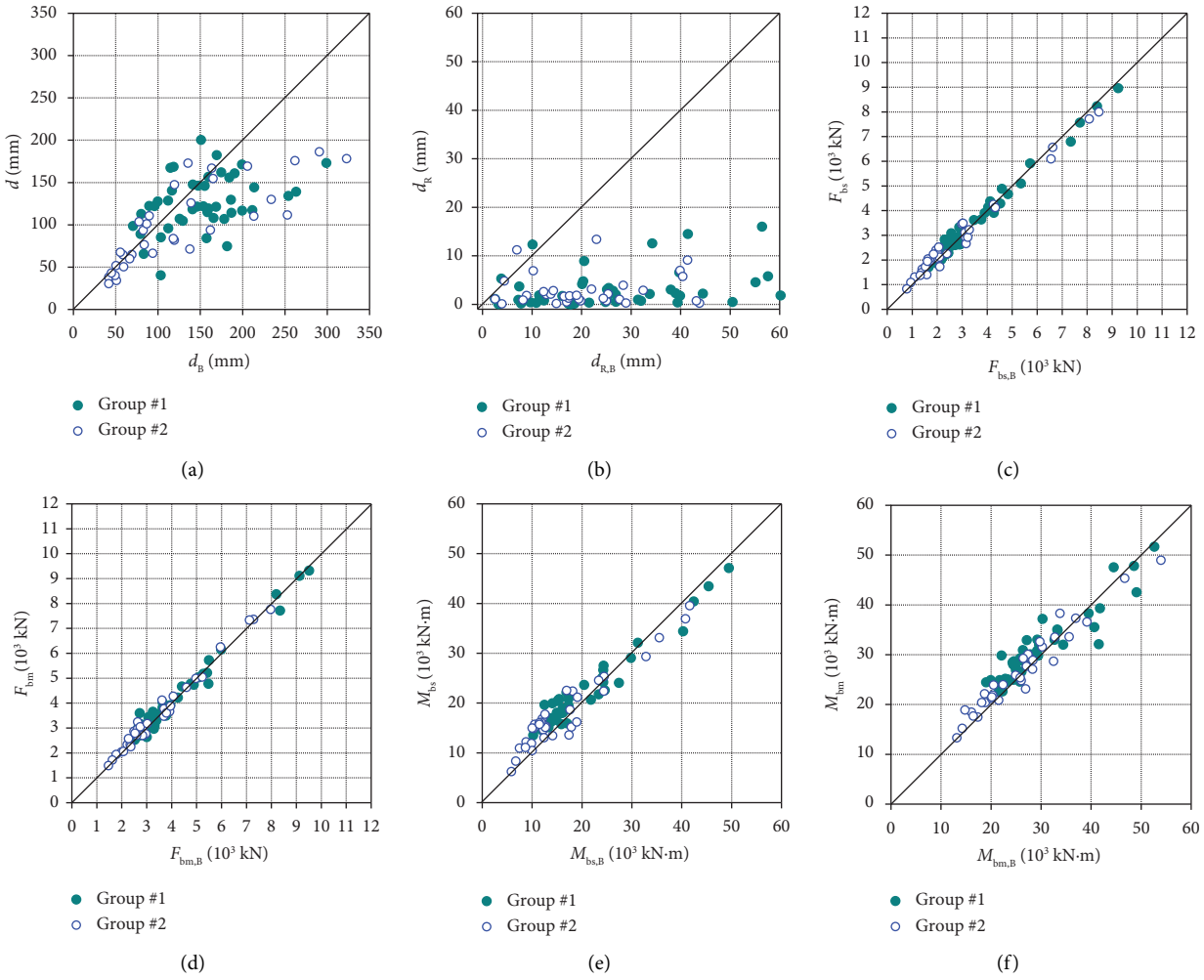

Figure 15: Response comparisons of SCFPI system with initial isolation period of 4.5 s, (a) d. (b) d_R. (c) F_{bs}. (d) F_{bm} in pier #2. (e) M_{bs}. (f) M_{bm} in pier #2.

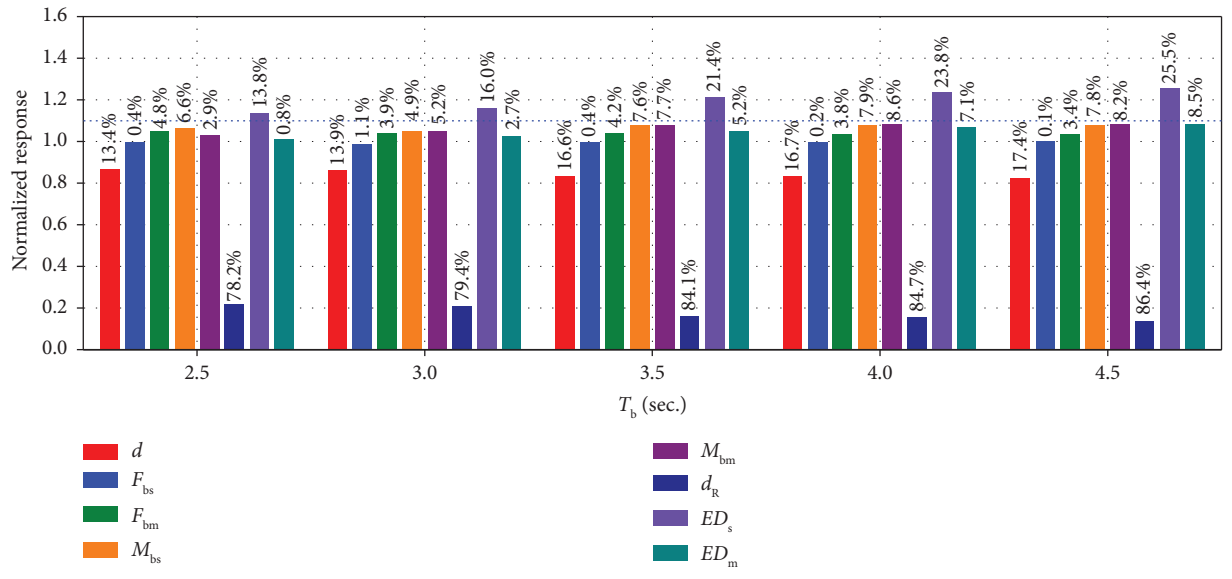

Figure 16: Continued.

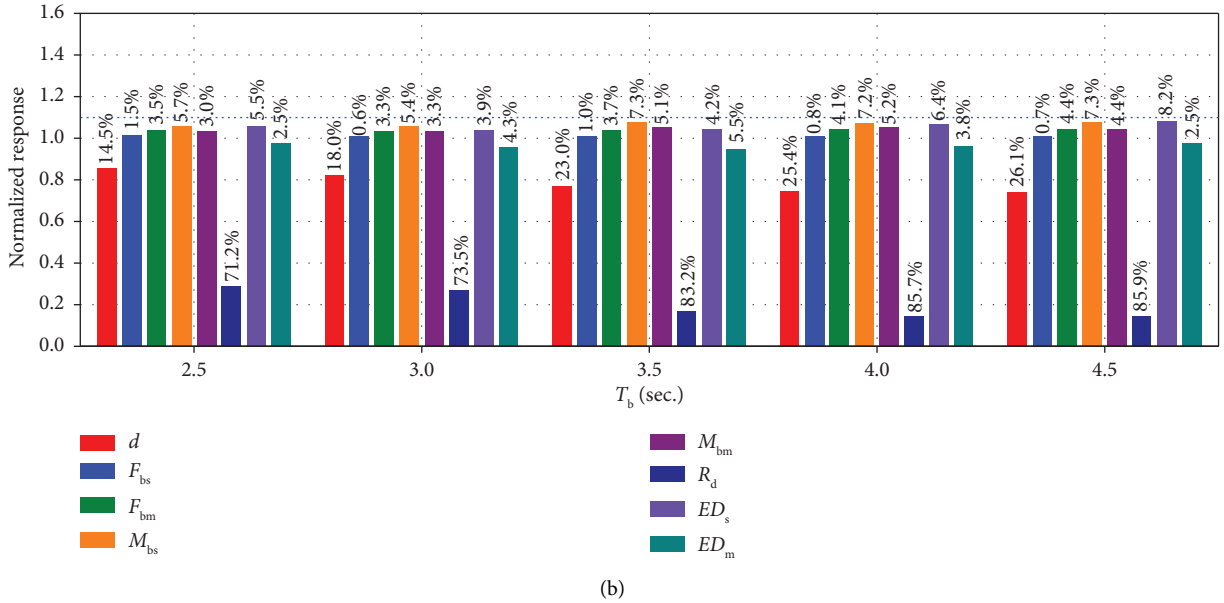

(b)

Figure 16: Normalized mean responses of the SCFPI systems. (a) Group-1. (b) Group-2.

study demonstrates the effectiveness of the cost-effective design method and response mitigation performance of the SCFPI system for bridges subjected to near-fault ground motions.

8. Conclusions

This paper develops a superelastic conical friction pendulum isolator (SCFPI) for seismic performance enhancement of bridges under near-fault ground motions. A cost-effective design method is developed to search the optimum SCFPI parameters. The usability of the proposed design method and the response control efficacy of the SCFPI system for bridges are demonstrated by conducting case studies, which provide a reliable basis to understand the response control efficiency of the bridge with SCFPIs and can also be utilized to guidefuture experimental studies. The achieved conclusions and suggestions are summarized as follows.

(i) The novel SCFPI can achieve effective adaptability and seismic performance enhancement of bridges under near-fault ground motions, e.g., mitigating the girder displacement and residual isolator displacement and controlling the increments of base forces in piers as well as enhancing the damping capacity.

(ii) The cost-effective design method is particularly effective to capture the parameters of the SCFPI system with different initial isolation periods. The cost-effective amount of the SMA is achieved by balancing the increments of the base forces in piers. The proposed method with resilient design is also feasible to design the SCFPI system for different types of large-span structures.

(iii) Case studies demonstrate the response control effectiveness of bridge with SCFPI system designed by the proposed design method. The seismic control efficacy reveals that the proposed design method can achieve the cost-effective design target, e.g., the girder displacement and residual isolator displacement show maximum mitigations of 26.1% and 85.9% under group #2 records, respectively. The peak increments of the base forces of the piers are all less than 8.6%. The maximum damping enhancement of the side SCFPI reaches 25.5%. The SCFPI system upgrades the seismic resilience of brides by minimizing pier damage.

(iv) The SCFPI system and the cost-effective design method employing a resilient design concept provide the isolation design framework for bridges with SCFPIs. The findings of this study offer a clear guidance for potential researchers and engineers and facilitate the applications in bridge performance upgrading.

Although the seismic performance of bridge isolated by SCFPIs has been numerically investigated by employing the experimentally obtained parameters [46, 61] and has obtained some meaningful conclusions, further testing investigations are necessary to validate the hysteretic behavior of the SCFPI and calibrate the developed numerical models in future. The seismic performance of a scaled bridge isolated by SCFPIs is needed to be further experimentally investigated and the experimental data can be employed to validate the numerical results. A comparative study will also be conducted to demonstrate the superiority of the SCFPI system compared to other isolation systems, e.g., the FP system in future.

Data Availability

The data used to support the findings of this study are available from the corresponding author upon request.

Conflicts of Interest

The authors declare that they have no conflicts of interest.

Authors' Contributions

Wenzhi Zheng carried out conceptualization, methodology, software, validation, investigation, data curation, writing-original draft, and funding acquisition. Ping Tan carried out the methodology, supervision, writing-review and editing, and funding acquisition. Jian Li carried out the methodology, supervision, and writing-review and editing. Hao Wang carried out the supervision and writing-review and editing. Yanhui Liu carried out the writing-review and editing, and funding acquisition. Zhibin Xian carried out the investigation, writing-review and editing.

Acknowledgments

The research was financially supported by the National Natural Science Foundation of China (Grant nos. 52108278 and 51978185), National Key R&D Program of China (Grant no. 2021YFE0112200), China Postdoctoral Science Foundation (Grant no. 2021M700925), Guangdong Basic and Applied Basic Research Foundation (Grant nos. 2023A1515012681 and 2021A1515010586), and Program for Changjiang Scholars and IRT in University (Grant no. IRT13057). The authors also would like to thank the Pacific Earthquake Engineering Research Center for providing the available data.

References

[1] P. Tsopelas and M. C. Constantinou, "NCEER-Taisei corporation research program on sliding seismic isolation systems for bridges: experimental and analytical study of a system consisting of sliding bearings and fluid restoring force/damping devices," State Univ. of New York at Buffalo, Buffalo, NY, USA, 1994.

[2] V. A. Zayas and S. S. Low, "Seismic isolation of bridges using friction pendulum bearings," in *Proceedings of the Structural engineering in the 21st century 1999 Structures Congress*, Struct Cong, New Orleans, Louisiana, April 1999.

[3] A. K. Agrawal, P. Tan, S. Nagarajaiah, and J. Zhang, "Benchmark structural control problem for a seismically excited highway bridge-Part I: phase I problem definition," *Structural Control and Health Monitoring*, vol. 16, no. 5, pp. 509–529, 2009.

[4] P. Tan and A. K. Agrawal, "Benchmark structural control problem for a seismically excited highway bridge-part II: phase I sample control designs," *Structural Control and Health Monitoring*, vol. 16, no. 5, pp. 530–548, 2009.

[5] N. Makris, "Seismic isolation: early history," *Earthquake Engineering & Structural Dynamics*, vol. 48, no. 2, pp. 269–283, 2019.

[6] H. Sheikh, N. C. Van Engelen, and R. Ruparathna, "A review of base isolation systems with adaptive characteristics," *Structures*, vol. 38, pp. 1542–1555, 2022.

[7] J. Shen, M. H. Tsai, K. C. Chang, and G. C. Lee, "Performance of a seismically isolated bridge under near-fault earthquake ground motions," *Journal of Structural Engineering*, vol. 130, no. 6, pp. 861–868, 2004.

[8] W. Z. Zheng, H. Wang, P. Tan, J. Li, and Y. H. Liu, "Numerical modeling and experimental validation of Sliding-LRBs considering hysteretic strength degradation," *Engineering Structures*, vol. 262, Article ID 114374, 2022.

[9] M. Dolce, D. Cardone, and G. Palermo, "Seismic isolation of bridges using isolation systems based on flat sliding bearings," *Bulletin of Earthquake Engineering*, vol. 5, no. 4, pp. 491–509, 2007.

[10] G. Sachdeva, S. Chakraborty, and S. Ray-Chaudhuri, "Seismic response control of a structure isolated by flat sliding bearing and nonlinear restoring spring: experimental study for performance evaluation," *Engineering Structures*, vol. 159, pp. 1–13, 2018.

[11] Y. B. Peng, L. C. Ding, and J. B. Chen, "Performance evaluation of base-isolated structures with sliding hydromagnetic bearings," *Structural Control and Health Monitoring*, vol. 26, no. 1, Article ID e2278, 2019.

[12] K. L. Ryan and A. K. Chopra, "Estimating the seismic displacement of friction pendulum isolators based on non-linear response history analysis," *Earthquake Engineering and Structural Dynamics*, vol. 33, no. 3, pp. 359–373, 2004.

[13] T. A. Morgan and S. A. Mahin, "Achieving reliable seismic performance enhancement using multi-stage friction pendulum isolators," *Earthquake Engineering & Structural Dynamics*, vol. 39, no. 13, pp. 1443–1461, 2010.

[14] W. Z. Zheng, H. Wang, J. Li, and H. J. Shen, "Parametric study of SMA-based friction pendulum system for response control of bridges under near-fault ground motions," *Journal of Earthquake Engineering*, vol. 25, no. 8, pp. 1494–1512, 2021.

[15] J. Shang, P. Tan, Y. Zhang, J. Han, and J. Qin, "Experimental and analytical investigation of variable friction pendulum isolator," *Engineering Structures*, vol. 243, Article ID 112575, 2021.

[16] P. Castaldo and G. Amendola, "Optimal sliding friction coefficients for isolated viaducts and bridges: a comparison study," *Structural Control and Health Monitoring*, vol. 28, no. 12, Article ID e2838, 2021.

[17] P. Castaldo and G. Amendola, "Optimal DCFP bearing properties and seismic performance assessment in non-dimensional form for isolated bridges," *Earthquake Engineering & Structural Dynamics*, vol. 50, no. 9, pp. 2442–2461, 2021.

[18] P. Castaldo, G. Amendola, L. Giordano, and E. Miceli, "Seismic reliability assessment of isolated multi-span continuous deck bridges," *Ingegneria Sismica-Int J Earthq Eng.*, vol. 39, no. 3, 2022.

[19] P. M. Calvi and G. M. Calvi, "Historical development of friction-based seismic isolation systems," *Soil Dynamics and Earthquake Engineering*, vol. 106, pp. 14–30, 2018.

[20] G. C. Lee, Y. Kitane, and I. G. Buckle, "Literature review of the observed performance of seismically isolated bridges," *Research Progress and Accomplishments: Multidisciplinary Center for Earthquake Engineering Research*, pp. 51–62, 2001.

[21] M. Sarrazin, O. Moroni, C. Neira, and B. Venegas, "Performance of bridges with seismic isolation bearings during the Maule earthquake, Chile," *Soil Dynamics and Earthquake Engineering*, vol. 47, pp. 117–131, 2013.

[22] C. W. Roeder, "Proposed design method for thermal bridge movements," *Journal of Bridge Engineering*, vol. 8, no. 1, pp. 12–19, 2003.

[23] R. Kromanis, P. Kripakaran, and B. Harvey, "Long-term structural health monitoring of the Cleddau bridge: evaluation of quasi-static temperature effects on bearing movements," *Structure and Infrastructure Engineering*, vol. 12, no. 10, pp. 1342–1355, 2016.

[24] F. Mazza, "Effects of the long-term behaviour of isolation devices on the seismic response of base-isolated buildings," *Structural Control and Health Monitoring*, vol. 26, no. 4, Article ID e2331, 2019.

[25] C. S. Tsai, T. C. Chiang, and B. J. Chen, "Finite element formulations and theoretical study for variable curvature friction pendulum system," *Engineering Structures*, vol. 25, no. 14, pp. 1719–1730, 2003.

[26] L. Y. Lu, T. Y. Lee, and S. W. Yeh, "Theory and experimental study for sliding isolators with variable curvature," *Earthquake Engineering & Structural Dynamics*, vol. 40, no. 14, pp. 1609–1627, 2011.

[27] W. Z. Zheng, P. Tan, Y. H. Liu, H. Wang, and H. T. Chen, "Multi-stage superelastic variable stiffness pendulum isolation system for seismic response control of bridges under near-fault earthquakes," *Structural Control and Health Monitoring*, vol. 29, no. 12, Article ID e3114, 2022.

[28] G. Auad and J. L. Almazán, "Evaluating the use of variable curvature frictional isolators to mitigate the adverse effects of internal lateral impacts," *Engineering Structures*, vol. 266, Article ID 114619, 2022.

[29] G. Auad, P. Castaldo, and J. L. Almazán, "Seismic reliability of structures equipped with LIR-DCFP bearings in terms of superstructure ductility and isolator displacement," *Earthquake Engineering & Structural Dynamics*, vol. 51, no. 13, pp. 3171–3214, 2022.

[30] L. Y. Lu, M. H. Shih, and C. Y. Wu, "Near-fault seismic isolation using sliding bearings with variable curvatures," in *Proceedings of the 13th World Conference on Earthquake Engineering*, Vancouver, B.C., Canada, August 2004.

[31] A. A. Shaikhzadeh and A. Karamoddin, "Effectiveness of sliding isolators with variable curvature in near-fault ground motions," *The Structural Design of Tall and Special Buildings*, vol. 25, no. 6, pp. 278–296, 2016.

[32] H. A. Admane and P. Murnal, "Comparative analysis of SIVC systems using simplified analytical modeling for practical design," *Practice Periodical on Structural Design and Construction*, vol. 26, no. 1, Article ID 04020051, 2021.

[33] C. Y. Yang, S. J. Wang, C. K. Lin, L. L. Chung, and M. C. Liou, "Analytical and experimental study on sloped sliding-type bearings," *Structural Control and Health Monitoring*, vol. 28, no. 11, Article ID e2828, 2021.

[34] W. Z. Zheng, H. Wang, H. Hao, K. M. Bi, and H. J. Shen, "Performance of bridges isolated with sliding-lead rubber bearings subjected to near-fault earthquakes," *International Journal of Structural Stability and Dynamics*, vol. 20, no. 2, Article ID 2050023, 2020.

[35] W. Zheng, H. Wang, H. Hao, and K. Bi, "Superelastic CuAlBe wire-based sliding lead rubber bearings for seismic isolation of bridges in cold regions," *Engineering Structures*, vol. 247, Article ID 113102, 2021.

[36] E. Ghafoori, B. Wang, and B. Andrawes, "Shape memory alloys for structural engineering: an editorial overview of research and future potentials," *Engineering Structures*, vol. 273, Article ID 115138, 2022.

[37] H. Qian, H. Li, and G. Song, "Experimental investigations of building structure with a superelastic shape memory alloy friction damper subject to seismic loads," *Smart Materials and Structures*, vol. 25, no. 12, Article ID 125026, 2016.

[38] Z. H. Zhang, K. M. Bi, H. Hao, P. Sheng, L. Feng, and D. Xiao, "Development of a novel deformation-amplified shape memory alloy-friction damper for mitigating seismic responses of RC frame buildings," *Engineering Structures*, vol. 216, Article ID 110751, 2020.

[39] C. Qiu, C. Fang, D. Liang, X. Du, and M. C. Yam, "Behavior and application of self-centering dampers equipped with buckling-restrained SMA bars," *Smart Materials and Structures*, vol. 29, no. 3, Article ID 035009, 2020.

[40] F. Casciati, L. Faravelli, and R. Al Saleh, "An SMA passive device proposed within the highway bridge benchmark," *Structural Control and Health Monitoring*, vol. 16, no. 6, pp. 657–667, 2009.

[41] J. Dong, C. S. Cai, and A. M. Okeil, "Overview of potential and existing applications of shape memory alloys in bridges," *Journal of Bridge Engineering*, vol. 16, no. 2, pp. 305–315, 2011.

[42] W. Zheng, H. Wang, J. Li, and H. Shen, "Parametric study of superelastic-sliding LRB system for seismic response control of continuous bridges," *Journal of Bridge Engineering*, vol. 25, no. 9, Article ID 04020062, 2020.

[43] C. Fang, D. Liang, Y. Zheng, and S. Lu, "Seismic performance of bridges with novel SMA cable-restrained high damping rubber bearings against near-fault ground motions," *Earthquake Engineering & Structural Dynamics*, vol. 51, no. 1, pp. 44–65, 2021.

[44] J. Deng, F. Hu, O. E. Ozbulut, and S. Cao, "Verification of multi-level SMA/lead rubber bearing isolation system for seismic protection of bridges," *Soil Dynamics and Earthquake Engineering*, vol. 161, Article ID 107380, 2022.

[45] B. Wang, S. Zhu, and F. Casciati, "Experimental study of novel self-centering seismic base isolators incorporating superelastic shape memory alloys," *Journal of Structural Engineering*, vol. 146, no. 7, Article ID 04020129, 2020.

[46] W. Z. Zheng, P. Tan, Z. H. Zhang, H. Wang, and Z. Sun, "Damping enhanced novel re-centering seismic isolator incorporating superelastic SMA for response control of bridges under near-fault earthquakes," *Smart Materials and Structures*, vol. 31, no. 6, Article ID 065015, 2022.

[47] O. E. Ozbulut and S. Hurlebaus, "Optimal design of superelastic-friction base isolators for seismic protection of highway bridges against near-field earthquakes," *Earthquake Engineering & Structural Dynamics*, vol. 40, no. 3, pp. 273–291, 2011.

[48] G. Attanasi and F. Auricchio, "Innovative superelastic isolation device," *Journal of Earthquake Engineering*, vol. 15, no. 1, pp. 72–89, 2011.

[49] D. Cardone, P. Narjabadifam, and D. Nigro, "Shaking table tests of the smart restorable sliding base isolation system (SRSBIS)," *Journal of Earthquake Engineering*, vol. 15, no. 8, pp. 1157–1177, 2011.

[50] H. Soul and A. Yawny, "Applicability of superelastic materials in seismic protection systems: a parametric study of performance in isolation of structures," *Smart Materials and Structures*, vol. 26, no. 8, Article ID 085036, 2017.

[51] D. Liang, Y. Zheng, C. Fang, M. C. H. Yam, and C. Zhang, "Shape memory alloy (SMA)-cable-controlled sliding bearings: development, testing, and system behavior," *Smart Materials and Structures*, vol. 29, no. 8, Article ID 085006, 2020.

[52] Y. Pang, W. He, and J. Zhong, "Risk-based design and optimization of shape memory alloy restrained sliding bearings for highway bridges under near-fault ground motions," *Engineering Structures*, vol. 241, Article ID 112421, 2021.

[53] S. Gur, G. N. Frantziskonis, and S. K. Mishra, "Thermally modulated shape memory alloy friction pendulum (tmSMA-FP) for substantial near-fault earthquake structure protection," *Structural Control and Health Monitoring*, vol. 24, no. 11, Article ID e2021, 2017.

[54] D. De Domenico, E. Gandelli, and V. Quaglini, "Adaptive isolation system combining low-friction sliding pendulum bearings and SMA-based gap dampers," *Engineering Structures*, vol. 212, Article ID 110536, 2020.

[55] Q. Han, X. Liang, J. Wen, J. Zhang, X. Du, and Z. Wang, "Multiple-variable frequency pendulum isolator with high-performance materials," *Smart Materials and Structures*, vol. 29, no. 7, Article ID 075002, 2020.

[56] P. Zhuang, W. Wang, Y. Li, and M. Han, "Cyclic behavior of an adaptive seismic isolation system combining a double friction pendulum bearing and shape memory alloy cables," *Smart Materials and Structures*, vol. 30, no. 7, Article ID 075003, 2021.

[57] Y. Li, H. Ozek, and O. E. Ozbulut, "An adaptive friction isolation system for seismic response control of buildings," *Smart Materials and Structures*, vol. 31, no. 9, Article ID 095045, 2022.

[58] C. H. Loh, W. I. Liao, and J. F. Chai, "Effect of near-fault earthquake on bridges: lessons learned from Chi-Chi earthquake," *Earthquake Engineering and Engineering Vibration*, vol. 1, pp. 86–93, 2002.

[59] J. Yuan, Y. Wang, B. Zhan, X. Yuan, X. Wu, and J. Ma, "Comprehensive investigation and analysis of liquefaction damage caused by the Ms 7.4 Maduo earthquake in 2021 on the Tibetan Plateau, China," *Soil Dynamics and Earthquake Engineering*, vol. 155, Article ID 107191, 2022.

[60] Pacific Earthquake Engineering Research Center, *(PEERC) OpenSees-Version 2.5.0*, Open System for Earthquake Engineering Simulation, CA, Berkeley, 2016.

[61] M. Dolce, D. Cardone, and F. Croatto, "Frictional behavior of steel-PTFE interfaces for seismic isolation," *Bulletin of Earthquake Engineering*, vol. 3, no. 1, pp. 75–99, 2005.

[62] M. Constantinou, A. Mokha, and A. Reinhorn, "Teflon bearings in base isolation II: modeling," *Journal of Structural Engineering*, vol. 116, no. 2, pp. 455–474, 1990.

[63] Ministry of Transport of Prc. (Mtprc), *Friction Pendulum Seismic Isolation Bearing for Highway Bridges (JT/T 852-2013)*, China Communications Press, Beijing, 2013.

[64] R. S. Jangid, "Seismic response of isolated bridges," *Journal of Bridge Engineering*, vol. 9, no. 2, pp. 156–166, 2004.

[65] P. Castaldo, D. Gino, G. Bertagnoli, and G. Mancini, "Resistance model uncertainty in non-linear finite element analyses of cyclically loaded reinforced concrete systems," *Engineering Structures*, vol. 211, Article ID 110496, 2020.

[66] M. S. Günay and H. Sucuoğlu, "Predicting the seismic response of capacity-designed structures by equivalent linearization," *Journal of Earthquake Engineering*, vol. 13, no. 5, pp. 623–649, 2009.

[67] American Society of Civil Engineers (Asce), *Minimum Design Loads for Buildings and Other Structures*, Standard ASCE/SEI 7-05, Reston, VA, 2005.

[68] Ministry of Transport of Prc. (Mtprc), *Specifications For Seismic Design Of Highway Bridges (JTG/T 2231-01—2020)*, China Communications Press, Beijing, 2020.

[69] Ministry of Transport of Prc (Mtprc), *Series of Elastomeric Pad Bearings for Highway Bridges (JT/T 663-2006)*, China Communications Press, Beijing, 2006.

[70] B. Andrawes and R. Desroches, "Comparison between shape memory alloy seismic restrainers and other bridge retrofit devices," *Journal of Bridge Engineering*, vol. 12, no. 6, pp. 700–709, 2007.